Plant Communications
Research Article

CellPress
PARTNER JOURNAL

Three CNGC Family Members, CNGC5, CNGC6, and CNGC9, Are Required for Constitutive Growth of *Arabidopsis* Root Hairs as Ca^{2+}-Permeable Channels

Yan-Qiu Tan[1,2], Yang Yang[1,2], An Zhang[1,2], Cui-Fang Fei[1,2], Li-Li Gu[1,2], Shu-Jing Sun[1], Wei Xu[1], Lingling Wang[1], Hongtao Liu[1] and Yong-Fei Wang[1,*]

[1]National Key Laboratory of Plant Molecular Genetics, CAS Center for Excellence in Molecular Plant Sciences, Shanghai Institute of Plant Physiology and Ecology, Chinese Academy of Sciences, Shanghai 200032, China

[2]University of Chinese Academy of Sciences, Shanghai 200032, China

***Correspondence: Yong-Fei Wang (wangyongfei@sibs.ac.cn)**

https://doi.org/10.1016/j.xplc.2019.100001

ABSTRACT

The genetic identities of Ca^{2+} channels in root hair (RH) tips essential for constitutive RH growth have remained elusive for decades. Here, we report the identification and characterization of three cyclic nucleotide-gated channel (CNGC) family members, CNGC5, CNGC6, and CNGC9, as Ca^{2+} channels essential for constitutive RH growth in *Arabidopsis*. We found that the *cngc5-1cngc6-2cngc9-1* triple mutant (designated *shrh1*) showed significantly shorter and branching RH phenotypes as compared with the wild type. The defective RH growth phenotype of *shrh1* could be rescued by either the expression of *CNGC5*, *CNGC6*, or *CNGC9* single gene or by the supply of high external Ca^{2+}, but could not be rescued by external K^+ supply. Cytosolic Ca^{2+} imaging and patch-clamp data in HEK293T cells showed that these three CNGCs all function as Ca^{2+}-permeable channels. Cytosolic Ca^{2+} imaging in growing RHs further showed that the Ca^{2+} gradients and their oscillation in RH tips were dramatically attenuated in *shrh1* compared with those in the wild type. Phenotypic analysis revealed that these three CNGCs are Ca^{2+} channels essential for constitutive RH growth, with different roles in RHs from the conditional player CNGC14. Moreover, we found that these three CNGCs are involved in auxin signaling in RHs. Taken together, our study identified CNGC5, CNGC6, and CNGC9 as three key Ca^{2+} channels essential for constitutive RH growth and auxin signaling in *Arabidopsis*.

Key words: Ca^{2+} channels, CNGC, root hair, polar growth, *Arabidopsis*

Tan Y.-Q., Yang Y., Zhang A., Fei C.-F., Gu L.-L., Sun S.-J., Xu W., Wang L., Liu H., and Wang Y.-F. (2020). Three CNGC Family Members, CNGC5, CNGC6, and CNGC9, Are Required for Constitutive Growth of *Arabidopsis* Root Hairs as Ca^{2+}-Permeable Channels. Plant Comm. **1**, 100001.

INTRODUCTION

Root hairs (RHs) are tubular-shaped structures resulted from the outgrowth of root epidermal cells. RHs greatly increase the overall surface area of roots and are essential for the acquisition of diverse ion nutrients and water as well as the interaction between plants and rhizosphere microbes (Cui et al., 2017; Ibáñez et al., 2017). The developmental process of RHs can be roughly categorized into three steps: cell-fate determination, RH initiation, and elongating polar growth. The cell fate of root epidermis is determined mainly by an intrinsic transcriptional factor network to be either hair (H) cells or non-hair (N) cells. In this transcriptional factor network, negative regulator GL2 (GLABRA2) is the central component (Rerie et al., 1994; Di Cristina et al., 1996; Berger et al., 1998; Lin and Schiefelbein, 2001). A transcriptional factor complex composed of GL2 (GLABRA2), EGL3 (ENHANCER OF GLABRA3), WER (WEREWOLF), and TTG1 (TRANSPARENT TESTA GLABRA1) positively regulates the expression of *GL2*, and the accumulation of GL2 protein represses H cell differentiation and leads to N cell fate (Hung et al., 1998; Lee and Schiefelbein,

Published by the Plant Communications Shanghai Editorial Office in association with Cell Press, an imprint of Elsevier Inc., on behalf of CSPB and IPPE, CAS.

1999; Walker et al., 1999; Bernhardt et al., 2003, 2005), whereas CPC (CAPRICE) and several redundant players function as negative regulators of GL2 (Wada et al., 1997, 2002; Schellmann et al., 2002; Kirik et al., 2004; Simon et al., 2007). RH initiation is a process of cell-wall loosening and bulge/swelling formation in the epidermal cells adopting H cell fate. External acidification and the production of reactive oxygen species (ROS) facilitate cell-wall loosening during RH initiation and tip growth (Bibikova et al., 1998; Liszkay et al., 2004; Monshausen et al., 2007). The local assembly of F-actin initiates bulge formation, and supports sustained tip growth of RHs (Baluska et al., 2000). A number of components, including ROS, a few small guanosine 5′-triphosphate (GTP)-binding proteins from ROP (Rho-related GTPase from plant) family, receptor-like kinase FERONIA (FER), and guanine nucleotide exchange factors (ROPGEFs), are involved in RH initiation and tip growth (Wymer et al., 1997; Molendijk et al., 2001; Foreman et al., 2003; Duan et al., 2010; Huang et al., 2013). The production of ROS triggers external Ca^{2+} influx and cytosolic Ca^{2+} elevation during RH initiation. It is believed that ROS production is required for RH initiation, but ROS-induced cytosolic Ca^{2+} elevation is not (Wymer et al., 1997; Foreman et al., 2003).

Tip growth of RHs is a process of exocytosis and cytoplasmic restructuring (Ketelaar et al., 2008; Rounds and Bezanilla, 2013), which is regulated by a complex machinery composed of diverse components, including cytoskeleton of F-actin and microtubules, ROP proteins, ROS, and cytosolic Ca^{2+} signaling (Pei et al., 2012; Grierson et al., 2014). The cytosolic Ca^{2+} gradient starts from the elevation of cytosolic Ca^{2+} during RH initiation in epidermis, and the high cytosolic Ca^{2+} area enters RHs after RH initiation to form a Ca^{2+} gradient in RH apex. The Ca^{2+} gradient functions as a key regulator of RH growth and orientation similar to its functions in other tip-growing cells, including pollen tubes, fungal hyphae, and neurons (Konrad et al., 2011; Guan et al., 2013; Akiyama and Kamiguchi, 2015), and the Ca^{2+}-sensitive components of the complex machinery for tip growth regulation can be the targets of Ca^{2+} signaling, including F-actin binding proteins, microtubule binding proteins, myosin XI motors, and ROPs (Bibikova et al., 1999; Baluska et al., 2000; Molendijk et al., 2001; Sieberer et al., 2005; Tominaga et al., 2012). Early studies revealed that the presence and oscillation of the Ca^{2+} gradient at RH tips are required for the tip growth and orientation of RHs (Bibikova et al., 1997; Felle and Hepler, 1997; Wymer et al., 1997; Monshausen et al., 2008), and that external Ca^{2+} influx through inward Ca^{2+} channels in the plasma membrane at RH tips is the main source of Ca^{2+} for the establishment, maintenance, and regulation of the Ca^{2+} gradients (Schiefelbein et al., 1992; Herrmann and Felle, 1995; Felle and Hepler, 1997; Wymer et al., 1997). Therefore, plasma membrane Ca^{2+} channels at RH tips become key components for the regulation of the Ca^{2+} gradients, RH tip growth, and orientation. However, the identities of the Ca^{2+} channels have remained largely unknown for decades. Electrophysiological analysis has detected the activity of three types of Ca^{2+} channels in *Arabidopsis* root epidermis and RHs, including Ca^{2+}-permeable non-selective cation channels (NSCCs), hyperpolarization-activated Ca^{2+} channels (HACCs), and depolarization-activated Ca^{2+} channel (DACCs) (Kiegle et al., 2000; Véry and Davies, 2000; Demidchik et al., 2002; Miedema et al., 2008). A model has been proposed that NSCCs and HACCs co-exist in root epidermal cells (Demidchik et al., 2002), and HACCs and DACCs co-exist in RHs in *Arabidopsis* (Miedema et al., 2008). NSCC-mediated Ca^{2+} influx dominates in mature epidermal cells, whereas HACC-mediated Ca^{2+} influx predominates in RHs (Demidchik et al., 2002). Further research has detected the activity of hyperpolarization-activated Ca^{2+} channels in *Arabidopsis* RHs, which could be activated by NADPH oxidase AtRBOHC (RHD2)-dependent ROS accumulation (Foreman et al., 2003; Liszkay et al., 2004), and tip-localized ROP proteins and their negative regulator RhoGDI (RhoGTPase GDP dissociation inhibitor) function as upstream regulators of RHD2 in RH growth (Molendijk et al., 2001; Jones et al., 2002; Carol et al., 2005; Carol and Dolan, 2006). Efforts have been made to identify the Ca^{2+} channels essential for RH growth, and progress has been made in the analysis of annexin and cyclic nucleotide-gated channel (CNGC) families in *Arabidopsis*. Annexin1 is the first Ca^{2+}-permeable channel identified in RHs, which is an ROS-activated non-selective K^+- and Ca^{2+}-permeable cation channel in *Arabidopsis* (Laohavisit et al., 2012). Both hyperpolarized and depolarized voltage-activated channel currents were observed in *Arabidopsis* RH apical spheroplast, but no significant difference was observed between *ann1* mutant and wild type (Laohavisit et al., 2012). *Arabidopsis* mutant *cngc14-1* showed a conditional short-hair phenotype only when RHs grew in solid Murashige and Skoog (MS) medium, and did not show any detectable RH defect as compared with the wild type when RHs were exposed to air (Zhang et al., 2017). Arecent study reported that the *cngc5cngc9cngc14* triple mutant did not form any RHs under their experimental conditions (Brost et al., 2019), suggesting that CNGC5/9/14 are required for RH initiation. However, the Ca^{2+} channels essential for constitutive RH growth have not been identified yet. In this study, we report that three CNGC members, CNGC5, CNGC6, and CNGC9, function redundantly as Ca^{2+} channels essential for constitutive RH tip growth by maintaining and regulating a sharp cytosolic Ca^{2+} gradient and its oscillation in RH tips in *Arabidopsis*, which are different from the roles of the conditional player CNGC14 in RHs. We also found that CNGC5, CNGC6 and CNGC9 are involved in auxin signaling in RHs.

RESULTS

The *cngc5 cngc6 cngc9* Triple and *cngc5 cngc6 cngc9 cngc14* Quadruple Knockout Mutants Show Strong Defects in RH Growth

Pollen tubes and RHs are both tip-growing cells. We revealed that CNGC18 was the dominant Ca^{2+} channel for pollen germination, pollen tube growth, and orientation (Gao et al., 2016; Gu et al., 2017), and other groups recently observed RH-related phenotypes in a few *cngc* mutants in *Arabidopsis* (Zhang et al., 2017; Brost et al., 2019). Thus, we hypothesized that the Ca^{2+} channels essential for RH growth are composed of CNGC members in *Arabidopsis*. To test the hypothesis, we generated a set of transgenic *Arabidopsis* lines by introducing a β-glucuronidase (GUS) encoding gene driven by a native promoter of the 20 *CNGC* members. GUS staining results showed that *CNGC5*, *CNGC6*, *CNGC9*, and *CNGC14* were strongly expressed in RHs (Figure 1A), whereas the remaining

16 *CNGC* members were not obviously expressed in RHs (Supplemental Figure 1). We collected T-DNA insertional single mutants *cngc5-1*, *cngc6-2*, *cngc9-1*, and *cngc14-1* and double mutant *cngc5-1cngc6-2* (Supplemental Figure 2A) (Wang et al., 2013). *cngc5-1* and *cngc9-1* were confirmed as knockout mutants (Supplemental Figure 2B and 2C), and *cngc6-2* was a knockdown mutant (Supplemental Figure 2D) (Wang et al., 2013). *cngc14-1* was already known as a knockout mutant (Zhang et al., 2017). We then generated the double mutants *cngc5-1cngc9-1* and *cngc6-2cngc9-1* by crossing the related single mutants with each other, triple mutant *cngc5-1cngc6-2cngc9-1* by crossing *cngc5-1cngc9-1* with *cngc5-1cngc6-2*, and quadruple mutant *cngc5-1cngc6-2cngc9-1cngc14-1* by crossing *cngc5-1cngc6-2cngc9-1* with *cngc14-1*. We analyzed RH-related phenotypes in these single, double, triple, and quadruple mutants by analyzing the RHs exposed to air. We found that the RH lengths in the wild type, four single mutants, and three double mutants were similar to each other without significant difference (Figure 1B and 1C; Supplemental Figure 3A). However, the RHs of triple mutant *cngc5-1cngc6-2cngc9-1* and quadruple mutant *cngc5-1cngc6-2cngc9-1cngc14-1* were significantly shorter compared with that of the wild type, four single mutants, and three double mutants (Figure 1B and 1C). We thus designated the triple mutant *cngc5-1cngc6-2cngc9-1* and quadruple mutant *cngc5-1cngc6-2cngc9-1cngc14-1* as *shrh1* (*short root hair1*) and *shrh2*, respectively. The RHs were significantly shorter by 50.9% for *shrh1* and 54% for *shrh2* compared with the wild type. We further observed weak RH branching defective phenotype in three double mutants and strong RH branching defective phenotype in *shrh1* and *shrh2* (Figure 1D and 1E). The RH branching rates were 6.5% for *cngc5-1cngc6-2*, 14% for *cngc5-1cngc9-1*, 15% for *cngc6-2cngc9-1*, 60.2% for *shrh1*, and 63.2% for *shrh2* (Figure 1D). We rarely observed branched RH in the wild type and the four single mutants, which showed RH branching rates of lower than 0.1% (Figure 1D). RH density (RH number per millimeter root length) was not significantly altered in all the mutants compared with the wild type and each other (Supplemental Figure 3B). The diameters of RH trunk close to RH tips and the diameters of RH initiation area were obviously variable and significantly larger by 34% and 43% in *shrh1* mutant as compared with that in the wild type, respectively (Figure 1E; Supplemental Figure 3C and 3D). No RH rupturing phenotype was observed in all genotypes. Of note, RHs exposed to the air and located in 2-mm range of the RH zone (RHZ) of roots (Supplemental Figure 3E) were counted in these RH phenotype analyses, including RH length, density, and branching. Next, we mainly focused on CNGC5, CNGC6, and CNGC9 in further investigation, considering that the RH phenotypes of *shrh1* and *shrh2* were similar to each other.

To oversee the dynamic growth of RHs, we performed time-lapse experiments to monitor RH growth for no less than 300 min. A set of optical sections under bright field were captured each 1 min, and the set of sectioning images were automatically merged into a single picture by a computer using the software Leica Application Suite X (Leica, Germany). RHs growing at different angles were able to be seen clearly in the merged bright-field pictures. These data showed that *shrh1* RHs grew significantly slower and ceased growth earlier than wild type (Figure 1F and 1G; Supplemental Figure 4). The RH initiation zone (RHIZ) of roots (Supplemental Figure 3E) was selected for the time-lapse experiments in bright field for RHs.

To further test whether the defective RH phenotypes resulted from the mutations in CNGC5, CNGC6, and CNGC9, we generated rescued lines by expressing the *CNGC*s in *shrh1* mutant background under their native promoters. We selected two complemented (COM) lines for each of the three *CNGC*s, six rescued lines in total, namely *CNGC5-COM2* (*CNGC5-COMPLEMENTED2*), *CNGC5-COM5*, *CNGC6-COM1*, *CNGC6-COM2*, *CNGC9-COM15*, and *CNGC9-COM23*, for further analysis. The expression of *CNGC5*, *CNGC6*, and *CNGC9* in the COM lines was confirmed by qRT–PCR experiments (Supplemental Figure 2B–2D). We found that the average RH lengths of the six COM lines were significantly longer than that of *shrh1* and *shrh2* mutants, but similar to each other and that of wild type, single mutants, and double mutants (Figure 1B and 1C). The RH branching phenotype of *shrh1* was also dramatically repressed by the expression of the three *CNGCs* (Figure 1D). RH densities of the COM lines were similar to each other and that of wild type and all the mutants (Supplemental Figure 3B). These data confirmed that the RH phenotypes of *shrh1* mutant resulted from the mutations in *CNGC5*, *CNGC6*, and *CNGC9*.

We next generated overexpression (OE) lines by overexpressing the three *CNGC*s with an eGFP fused to their N terminus under control of the *Arabidopsis Ubiquitin10* promoter in the wild-type background. Two OE lines were selected for each *CNGC*, and six OE lines in total, namely *CNGC5-OE35* (*CNGC5-OVEREXPRESSION35*), *CNGC5-OE42*, *CNGC6-OE1*, *CNGC6-OE27*, *CNGC9-OE37*, and *CNGC9-OE42*, for experiments. The overexpression of *CNGC5*, *CNGC6*, and *CNGC9* in the OE lines was confirmed by qRT–PCR (Supplemental Figure 2B–2D). We found that the average RH lengths of *CNGC5-OE35*, *CNGC5-OE42*, *CNGC6-OE1*, and *CNGC6-OE27* were significantly longer than that of *shrh1* and *shrh2*, but similar to each other and that of wild type, single mutants, double mutants, and COM lines except *CNGC5-COM2* (Figure 1C). The average RH lengths were significantly increased in *CNGC9-OE37* and *CNGC9-OE42* compared with wild type, mutants, COM lines, and the remaining four OE lines (Figure 1C). Considering that CNGC9 rescued the RH phenotype of *shrh1* mutant to a similar extent as that of CNGC5 and CNGC6, the longer RHs in *CNGC9-OE37* and *CNGC9-OE42* implied that CNGC9 could play a slightly dominant role in RH growth relative to CNGC5 and CNGC6. We rarely observed branching RHs in all six OE lines (Figure 1D). The RH densities of the OE lines were not obviously altered relative to wild type, mutants, and COM lines (Supplemental Figure 3B). Together, these data demonstrate that CNGC5, CNGC6, and CNGC9 are required for tip growth of RHs in the air, in which CNGC9 plays a more important role than CNGC5 and CNGC6 in *Arabidopsis*.

CNGC5, CNGC6, and CNGC9 Are Predominantly Localized in the Periphery of RHs

We analyzed the subcellular localization of the three CNGCs by analyzing the eGFP fluorescent signal in the RHs of three OE lines *CNGC5-OE42*, *CNGC6-OE27*, and *CNGC9-OE42*, in which *eGFP-CNGC5*, *eGFP-CNGC6*, and *eGFP-CNGC9* were

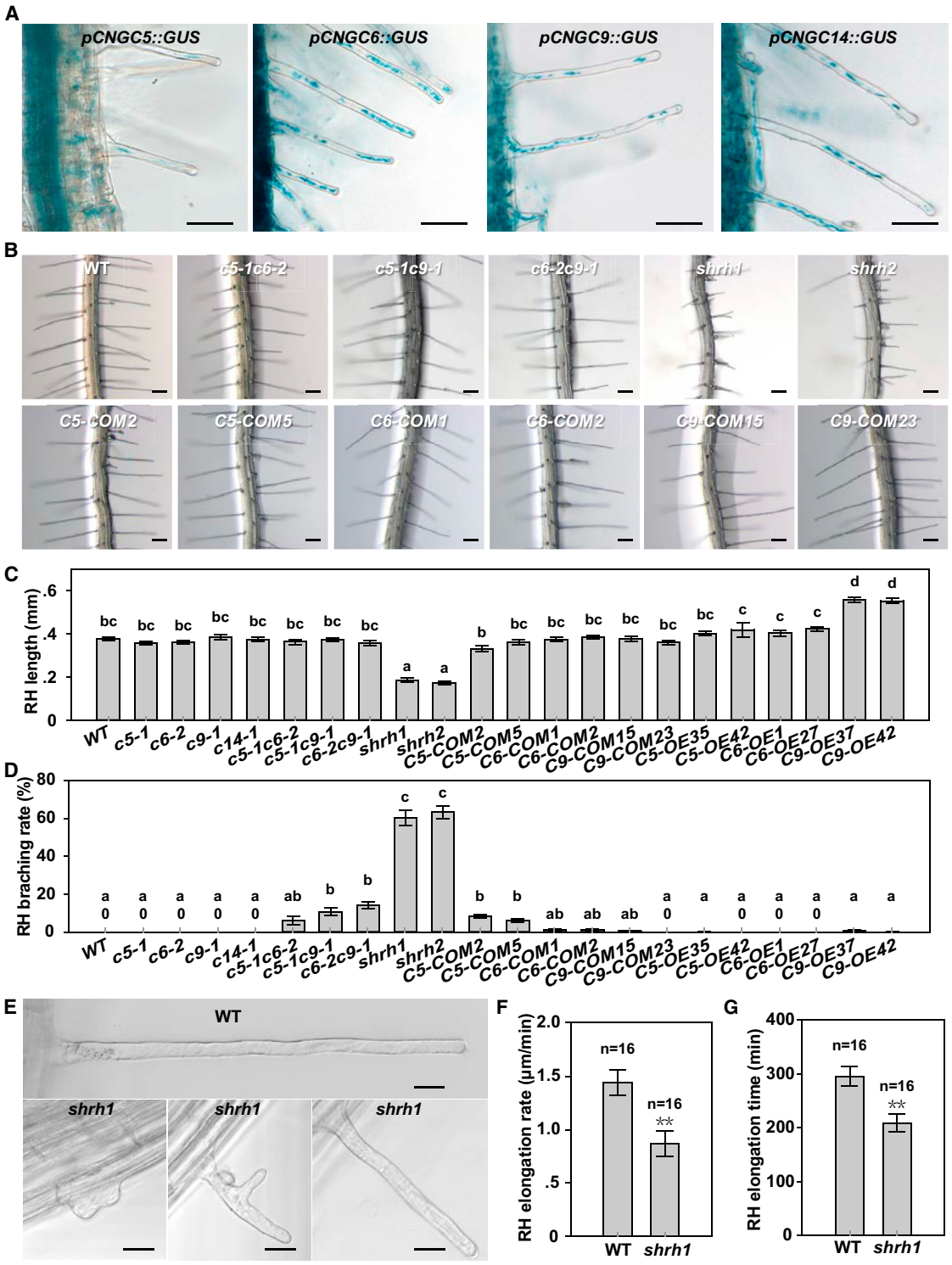

Figure 1. CNGC5, CNGC6, CNGC9, and CNGC14 Are Required for RH Growth in *Arabidopsis*.

(A) GUS staining results of CNGC5, CNGC6, CNGC9, and CNGC14 in RHs.

(B) Images of typical roots and hairs.

(C and D) Statistical analysis of RH length **(C)** and branching rate **(D)**.

(E) Images of typical RHs.

(F and G) Statistical analysis of elongation rate **(F)** and elongating time of RHs **(G)**.

(legend continued on next page)

overexpressed. However, we observed a dominant plasma membrane localization of the three CNGC proteins plus some distribution in cytoplasm (data not shown). The cytoplasm distribution of the three CNGC proteins could be a result of the overexpression of the three *CNGCs*. We thus analyzed the eGFP fluorescence distribution in three weaker OE lines, namely *CNGC5-OE4*, *CNGC6-OE12*, and *CNGC9-OE18*. We found that the eGFP fluorescent signal was distributed randomly in wild-type RHs (Supplemental Figure 5). However, the eGFP fluorescent signal was clearly distributed in the peripheral area of RHs (Supplemental Figure 5). Plasma membrane dye FM4-64 was then used to stain RHs, and an overlap of FM4-64 signal and eGFP fluorescence was clearly observed in the peripheral area in the merged photos, demonstrating a plasma membrane localization of the three CNGC proteins (Supplemental Figure 5).

The Defective RH Phenotypes in *Shrh1* Could Be Rescued by the Supply of High External Ca^{2+} Rather than K^+

The CNGC family has been predicted as NSCCs. Research from different groups revealed that CNGC2 and CNGC4 are permeable to both K^+ and Ca^{2+} (Leng et al., 1999, 2002; Wang et al., 2017), whereas several other CNGCs (including CNGC7, 8, 9, 10, 11, 12, 14, 16, and 18) are selective to Ca^{2+} (Urquhart et al., 2011; Gao et al., 2014, 2016; Zhang et al., 2017). The double mutant *cngc5-1cngc6-2* showed disrupted Mg^{2+}-permeable channel activity in *Arabidopsis* guard cells (Wang et al., 2013), suggesting that CNGC5 and CNGC6 are Ca^{2+}-permeable channels because most Ca^{2+} channels are permeable to diverse divalent cations, including Mg^{2+}, Ca^{2+}, and Ba^{2+}. Thus, we hypothesized that CNGC5, CNGC6, and CNGC9 function as inward Ca^{2+} channels in RHs. To test the hypothesis, we tested external Ca^{2+} dependence of RH growth. We found that RH growth was strongly impaired by the absence of external Ca^{2+} (no Ca^{2+} added) compared with control condition (3 mM external Ca^{2+} added), and RHs grew significantly longer when the external Ca^{2+} concentration ($[Ca^{2+}]_{ext}$) was increased to a higher concentration in all genotypes tested (Figure 2A and 2B). The RH branching rates were not obviously altered in wild type, *CNGC9-COM15*, and *CNGC9-OE42* upon the increases of $[Ca^{2+}]_{ext}$, but were significantly reduced in *shrh1* mutant relative to wild type, *CNGC9-COM15*, and *CNGC9-OE42* (Figure 2C). These data demonstrate that the shorter and branching RH phenotypes of *shrh1* resulted from reduced external Ca^{2+} influx, consistent with the Ca^{2+} dependence of RH growth (Schiefelbein et al., 1992). In addition, the promotion of RH growth by high external Ca^{2+} in wild type, *shrh1*, *CNGC9-COM15*, and *CNGC9-OE42* (Figure 2A and 2B) suggests the presence of other Ca^{2+} channels in RHs, and the significantly longer RHs of *CNGC9-OE42* relative to *CNGC9-COM15* and wild type in multiple external Ca^{2+} conditions (Figure 2B) support a dominant role of CNGC9 relative to CNGC5 and CNGC6 in RH growth. Moreover, we found that the RH densities were significantly reduced by the absence of external Ca^{2+} (no Ca^{2+} added), and significantly increased at the 15 mM $[Ca^{2+}]_{ext}$ condition compared with 3–10 mM $[Ca^{2+}]_{ext}$ condition in all the genotypes tested (Figure 2D), suggesting that RH initiation could be affected by low (0 mM) and high (15 mM) $[Ca^{2+}]_{ext}$ conditions relative to modest external Ca^{2+} conditions.

To test whether the three CNGCs were also involved in RH growth as K^+ channels by mediating external K^+ influx, we fixed external Ca^{2+} concentration at 3 mM, and analyzed the external K^+ dependence of RH length, branching, and density. We found that the average RH length, branching rate, and density were not obviously altered upon the increase of external K^+ concentration ($[K^+]_{ext}$) from micromolar level (no external K^+ added) (Xu et al., 2006) to 4 mM, 10 mM, 15 mM, and 20 mM in *shrh1* mutant, *CNGC9-COM15*, *CNGC9-OE42*, and wild type (Figure 3A–3D). However, the RHs were still significantly shorter in *shrh1* mutant and significantly longer in *CNGC9-OE42* compared with the wild type and *CNGC9-COM15* (Figure 3A and 3B), suggesting that the RH-related phenotypes in *shrh1* were not obviously related to K^+. Together, these data suggest that CNGC5, CNGC6, and CNGC9 function specifically as essential Ca^{2+} channels rather than K^+ channels in RH growth in *Arabidopsis*.

CNGC5, CNGC6, and CNGC9 Are Ca^{2+}-Permeable Channels

To characterize CNGC5, CNGC6, and CNGC9, we conducted cytosolic Ca^{2+} imaging experiments by transient expression in HEK293T cells. We observed a large cytosolic Ca^{2+} increase in HEK293T cells expressing one of the three *CNGCs* upon the application of 10 mM external Ca^{2+} (Figure 4A–4C), but only a small cytosolic Ca^{2+} increase was observed in some of the mock control HEK293T cells expressing *eGFP* (Figure 4D), suggesting that the three CNGCs are Ca^{2+}-permeable channels. HEK293T cells have an endogenous Ca^{2+} channel in the plasma membrane called CRACM1, which is specifically activated by the depletion of intracellular Ca^{2+} stores (Feske et al., 2006). It is not clear whether the small occasional Ca^{2+} increase in mock control HEK293T cells resulted from CRACM1-mediated external Ca^{2+} influx. However, CNGC-mediated cytosolic Ca^{2+} increases were clear and sharp without being obviously affected by the small and occasional background Ca^{2+} increase in HEK293T cells.

We next conducted patch-clamp experiments in HEK293T cell using Ca^{2+}-based standard bath and pipette solutions (Gao et al., 2014, 2016). HEK293T cells were transformed, and the transformed cells with eGFP fluorescence in the similar size were selected for patch-clamp analysis. We observed large inward Ca^{2+} channel currents in HEK293T cells expressing either *CNGC5* (Figure 4E and 4F) or *CNGC6* (Figure 4G and 4H), and these large channel currents were abolished upon the application of the Ca^{2+} channel blocker La^{3+} (100 μM) (Figure 4F and 4H). We observed only a small background conductance in mock control cells (Figure 4E–4H). To test

WT, wild type. See the figure legend of Supplemental Figure 3 for the annotation of genotypic initials of *Arabidopsis* lines. No less than 30 roots and 200 RHs (7–10 RHs per root) were counted for each analysis of each line. Error bars depict means ± SEM. Samples with different letters are significantly different with $P < 0.05$ (Kruskal–Wallis one-way ANOVA) in **(C)** and **(D)**. Letter n denotes the numbers of RH analyzed, and ** denotes significant difference with $P < 0.01$ (Mann–Whitney Rank Sum Test) in **(F)** and **(G)**. Scale bars, 0.05 mm **(A)**, 0.1 mm **(B)**, and 20 μm **(E)**.

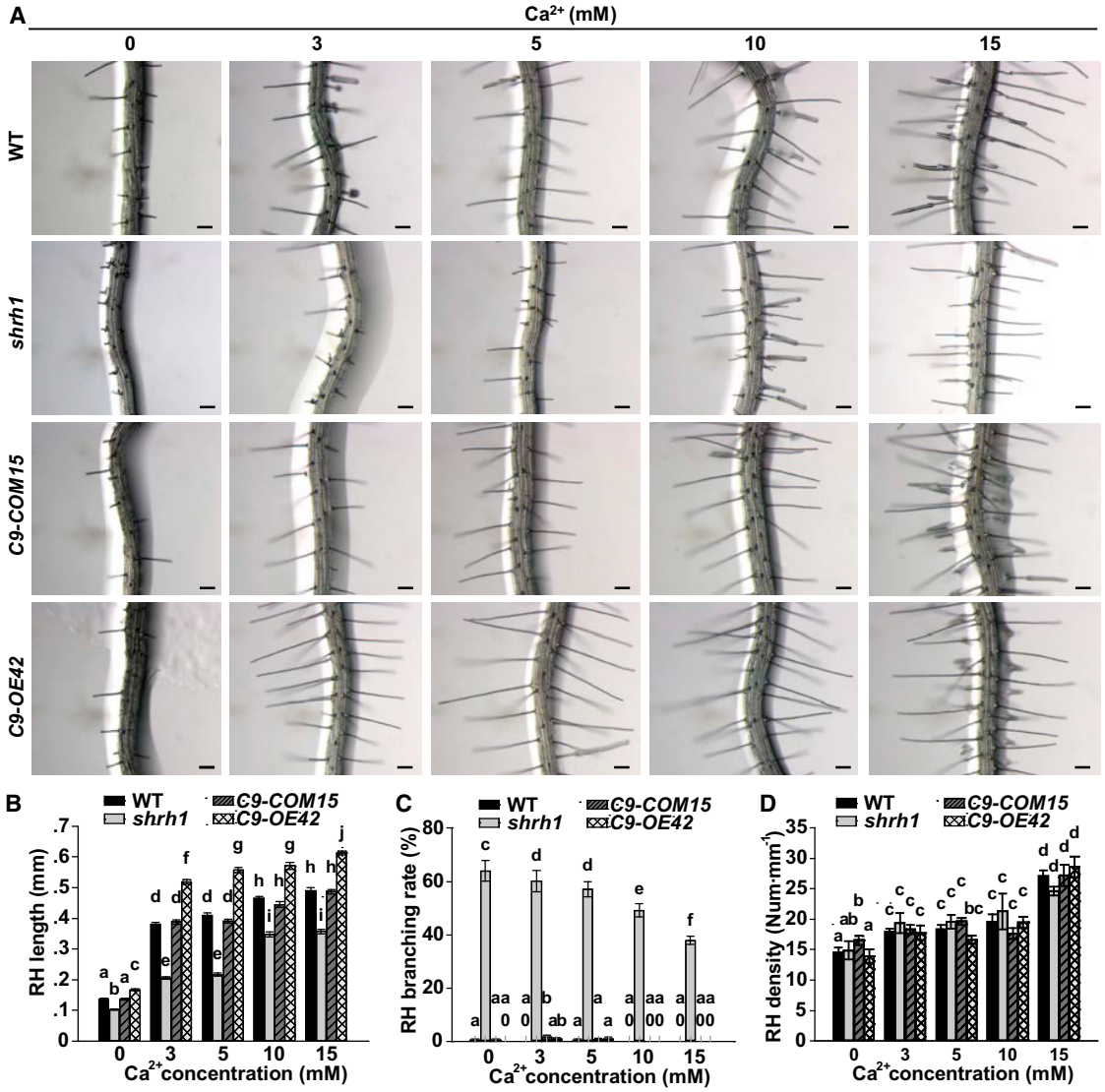

Figure 2. External Ca^{2+} Dependence of RH Growth in *Arabidopsis*.

(A) Images of typical roots and hairs. Scale bars, 0.1 mm.

(B–D) Average lengths **(B)**, branching rates **(C)**, and densities **(D)** of RHs at $[Ca^{2+}]_{ext}$ as indicated. *C9-COM15* and *C9-OE42* denote *CNGC9-COM15* and *CNGC9-OE42*, respectively. No less than 30 roots and 200 RHs (7-10 RHs per root) were analyzed for each analysis of each line. Error bars depict means ± SEM. Samples with different letters are significantly different with $P < 0.05$ (two-way ANOVA).

whether the inward channel currents were carried by Na^+ considering the presence of 120 mM Na^+ in the bath solution, we substituted Na^+ with the impermeant cation $NMDG^+$ (*N*-methyl-D-glucamine) in the bath solution, and kept the pipette solution unchanged. We pursued further patch-clamp experiments, and observed obvious inward channel currents in HEK293T cells expressing either *CNGC5* (Supplemental Figure 6A and 6B) or *CNGC6* (Supplemental Figure 6C and 6D). The inward channel currents were abolished upon the application of the Ca^{2+} channel blocker Gd^{3+} (100 μM) (Supplemental Figure 6A–6D). The large inward channel currents recorded in $NMDG^+$-based bath solution were similar to the currents recorded in Na^+-based bath solution, and the inhibitory effect of Gd^{3+} was similar to that of La^{3+} (Figure 4E–4H and Supplemental Figure 6). These data demonstrate that the inward channel currents recorded in HEK293T cells expressing either *CNGC5* or *CNGC6* were mainly carried by Ca^{2+}, not Na^+.

The cytosolic Ca^{2+} imaging data and patch-clamp data together demonstrate that CNGC5 and CNGC6 are Ca^{2+}-permeable channels. CNGC9 has been characterized as a Ca^{2+}-permeable channel in HEK293T cells using a patch-clamp technique (Gao et al., 2016). Thus, CNGC5, CNGC6, and CNGC9 are all Ca^{2+}-permeable channels.

Cytosolic Ca^{2+} Gradients in RH Tips Are Dramatically Attenuated in *Shrh1*

To investigate how CNGC5, CNGC6, and CNGC9 are involved in RH growth as Ca^{2+} channels *in vivo*, we generated transgenic *Arabidopsis* lines by introducing a construct containing

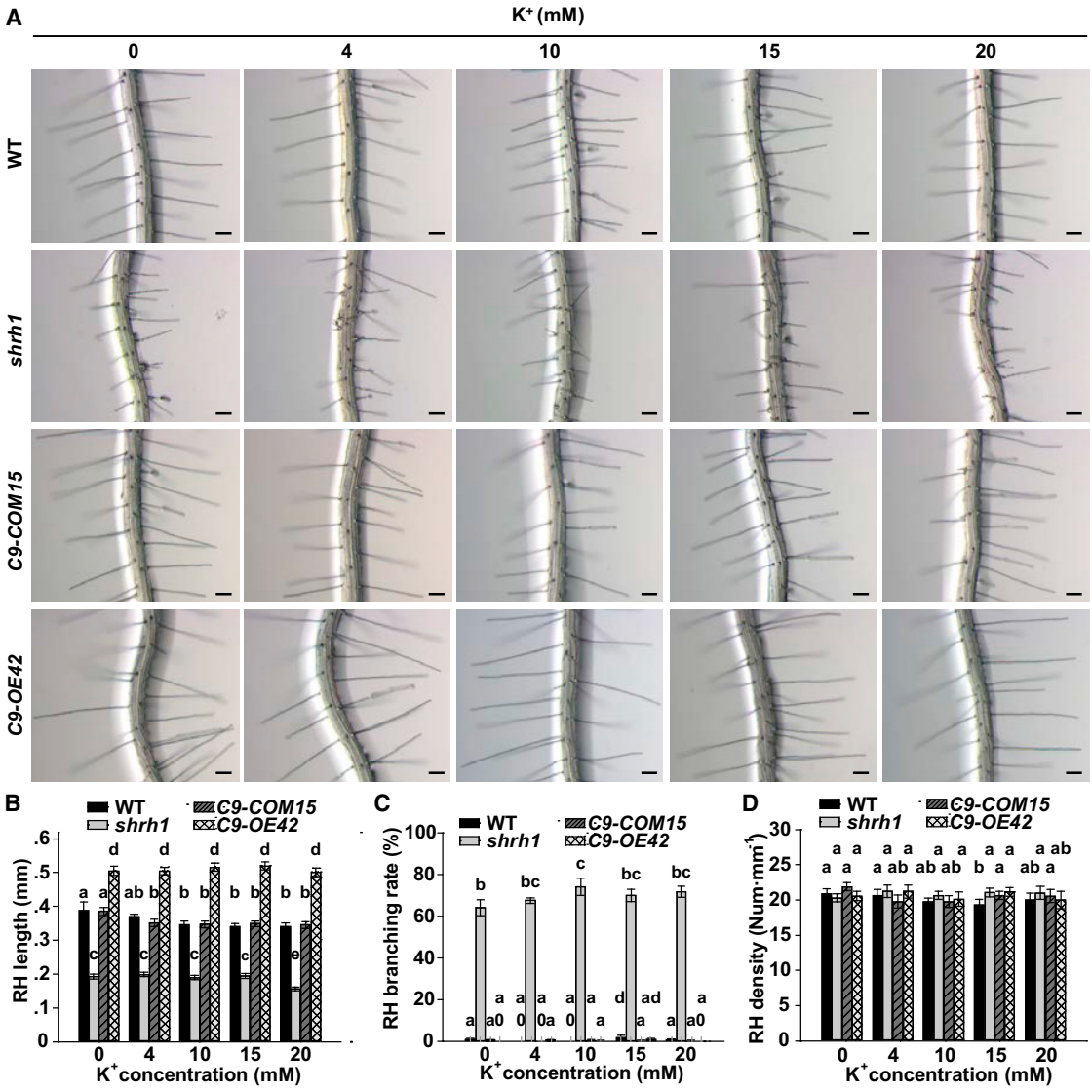

Figure 3. Defective RH Growth Phenotypes in *Shrh1* Are Independent of External K^+.

(A) Images of typical roots and hairs at external [K^+] as indicated. Scale bars, 0.1 mm.

(B–D) Statistical analysis of length **(B)**, branching rate **(C)**, and density **(D)** of RHs. *C9-COM15* and *C9-OE42* denote *CNGC9-COM15* and *CNGC9-OE42*, respectively. No less than 30 roots and 200 RHs (7-10 RHs per root) were analyzed for each analysis of each line. Error bars depict means ±SEM. Samples with different letters are significantly different with $P < 0.05$ (two-way ANOVA).

the Ca^{2+} indicator encoding gene of Yellow Cameleon version 3.6 (YC 3.6) under the control of *Arabidopsis Ubiquitin10* promoter into *shrh1* mutant and wild-type plants and performed time-lapse experiments to monitor the Ca^{2+} gradient and oscillation in growing RH tips. We observed not only a much stronger ratio signal of fluorescence resonance energy transfer (FRET)/CFP, but also a significantly sharper gradient of FRET/CFP in wild-type RH apex as compared with that in *shrh1* mutant throughout the whole oscillating growth phase (Figure 5A), suggesting that cytosolic Ca^{2+} gradients in *shrh1* RH tips were significantly reduced compared with those in the wild type. The vacuole regions were observed clearly in both wild-type and *shrh1* RHs, confirming the growth of the RHs (Supplemental Video 1).

We further analyzed the cytosolic Ca^{2+} oscillation in RH apex. The wild type and *shrh1* mutant RHs showed similar Ca^{2+} oscillation periods (Figure 5B). However, cytosolic Ca^{2+} oscillation in *shrh1* was much weaker compared with that of wild type (Figure 5B). Results similar to those shown in Figure 5 were observed in 15 out of 18 wild-type RHs tested and 12 out of 12 *shrh1* RHs tested. To test whether the weaker Ca^{2+} gradient and oscillation in *shrh1* RHs resulted from a lower expression of *YC3.6* relative to wild type, we conducted *in situ* $[Ca^{2+}]_{cyt}$ calibration (Swanson and Gilroy, 2013). Similar R_{min} and R_{max} were recorded in wild-type and *shrh1* RHs (Supplemental Figure 7A–7D), and the estimated $[Ca^{2+}]_{cyt}$ in *shrh1* was similar to that of wild type (Supplemental Figure 7E and 7F), suggesting that the expression of *YC3.6* in *shrh1* RHs was

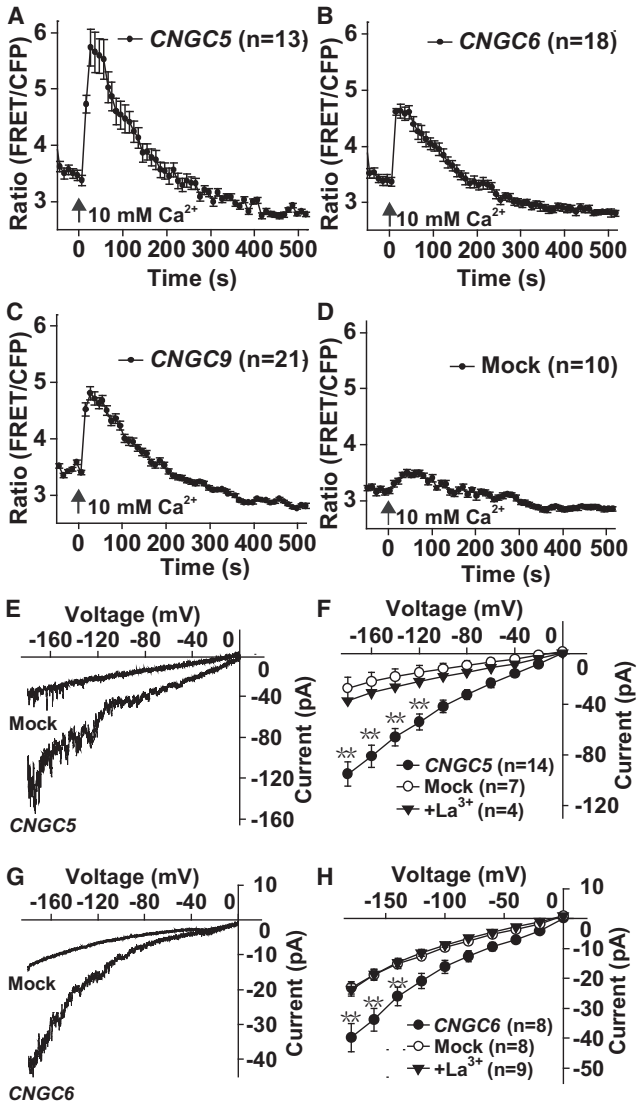

Figure 4. CNGC5, CNGC6, and CNGC9 Are Ca^{2+}-Permeable Channels.

(A–D) Cytosolic Ca^{2+} imaging data showing 10 mM Ca^{2+}-triggered cytosolic Ca^{2+} increases in HEK293T cells expressing *CNGC5* **(A)**, *CNGC6* **(B)**, and *CNGC9* **(C)** compared with the control HEK293T cells expressing *YC3.6* **(D)**.

(E–H) Patch-clamp analysis of CNGC5- and CNGC6-mediated channel currents in HEK293T cells. **(E and F)** Typical whole-cell recordings **(E)** and average current–voltage curves of steady-state whole-cell currents **(F)** recorded in HEK293T cells expressing either *CNGC5* or *eGFP*. **(G and H)** Typical whole-cell recordings **(G)** and average current–voltage curves of steady-state whole-cell currents **(H)** recorded in HEK293T cells expressing either *CNGC6* or *eGFP*.

Error bars depict means ± SEM. Letter n denotes the numbers of cells tested, and ** denotes significant difference with $P < 0.01$ (Kruskal–Wallis one-way ANOVA).

similar to that of wild type. These data together demonstrate that CNGC5, CNGC6, and CNGC9 are involved in RH growth by establishing and maintaining a sharp Ca^{2+} gradient and regulating the Ca^{2+} oscillation in RH apex, both of which are required for RH tip growth.

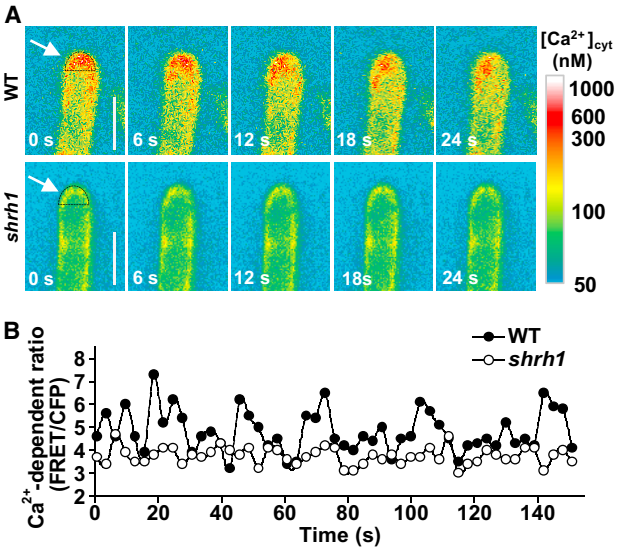

Figure 5. Cytosolic Ca^{2+} Oscillation in RH Tips Is Strongly Attenuated in *shrh1*.

(A) Typical time-elapses of RH images showing a sharp cytosolic Ca^{2+} gradient and its strong oscillation in wild type, and an attenuated Ca^{2+} gradient and its weaker oscillation in *shrh1* mutant in RH tips (left). A pseudocolor scale bar for relative cytosolic Ca^{2+} level calibration is shown on the right. Scale bars, 10 μm.

(B) Typical oscillation of FRET/CFP ratio of YC3.6 in RH tips in wild type and *shrh1* mutant. The white arrows in **(A)** show the regions of interest for Ca^{2+} oscillation measurement. Fifteen out of 18 wild-type RHs tested showed a sharp Ca^{2+} gradient and obvious Ca^{2+} oscillation in RH tips. Twelve out of 12 *shrh1* RHs tested showed much weaker Ca^{2+} gradient and oscillation relative to wild type.

CNGC5, CNGC6, and CNGC9 Are Essential for Constitutive Growth of RHs

It has been reported that *cngc14-1* mutant showed short RH phenotype only when RHs grew in solid medium, not in air (Zhang et al., 2017). The RH phenotypes observed in this research were mainly related to the RHs exposed to air. One possibility is that CNGC5, CNGC6, and CNGC9 function in one signaling pathway while CNGC14 functions in another. A second possibility is that CNGC5, CNGC6, and CNGC9 are Ca^{2+} channels essential for constitutive RH growth in all different conditions, whereas CNGC14 is only a conditional player. To test these possibilities, we analyzed the RH phenotypes when RHs grew in solid medium, not in air. The experimental results showed that the average RH lengths of *cngc14-1*, *shrh1*, and *shrh2* were similar to each other without significant difference, but significantly shorter compared with wild type (Figure 6A and 6B), demonstrating that the four CNGC members are all required for polar growth of RHs in solid medium. The RH branching rate was 66% for *shrh1* and 65% for *shrh2* in this experimental condition, which were similar to each other but significantly higher than that of wild type (0%) and *cngc14-1* mutant (0.04%) (Figure 6C), indicating that the RH branching phenotype we observed mainly resulted from the simultaneous mutations in *CNGC5*, *CNGC6*, and *CNGC9*, not *CNGC14*. We also observed ruptured RHs in solid medium, and the rupturing rates were zero for the wild type and *shrh1*, 80.9% for *cngc14-1*, and 86.6% for *shrh2* (Figure 6D),

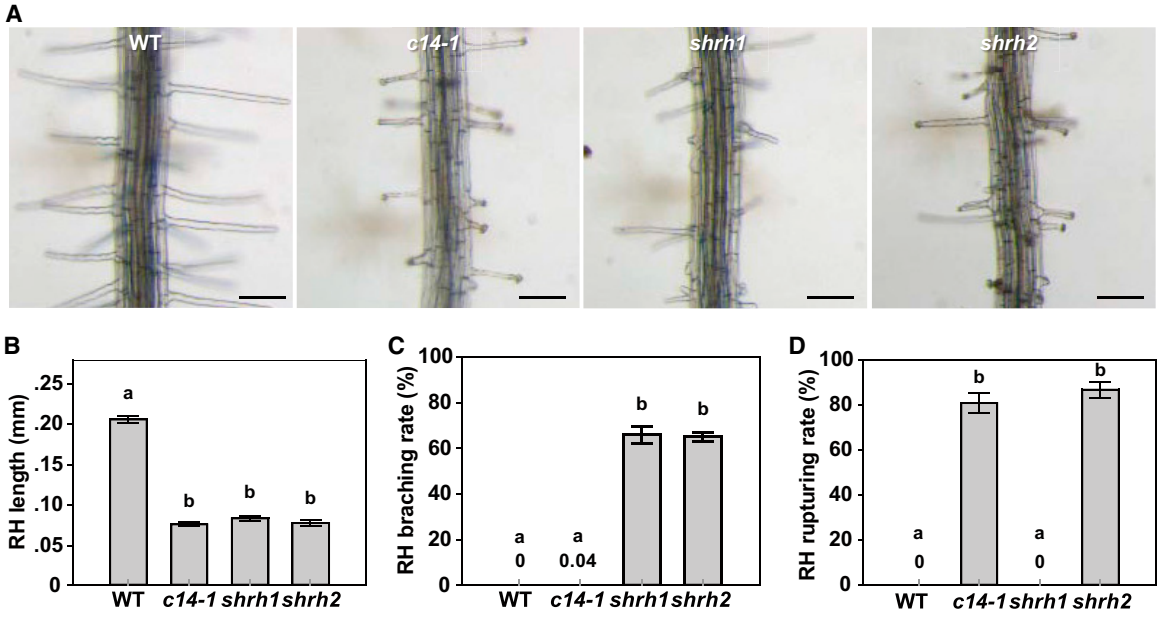

Figure 6. Phenotypic Analysis of *Arabidopsis* RHs Grown in Solid Medium.

(A) Images of typical roots and hairs. Scale bars, 0.1 mm.

(B–D) Statistical analysis of RH length **(B)**, branching rate **(C)**, and rupturing rate **(D)** of RHs. No less than 30 roots and 200 RHs (7–10 RHs per root) were counted for each analysis of each line. Error bars depict means ±SEM. Samples with different letters are significantly different with $P < 0.05$ (Kruskal–Wallis one-way ANOVA). See also Supplemental Figure 7 for RH density analysis.

suggesting that the RH rupturing phenotype in the condition we used mainly resulted from the mutation in *CNGC14*, not in *CNGC5*, *CNGC6*, and *CNGC9*. The wild-type, *cngc14-1*, *shrh1*, and *shrh2* plants showed similar RH density (Supplemental Figure 8), suggesting that all four CNGCs were not obviously involved in RH initiation under these conditions. These data together suggest that CNGC5, CNGC6, and CNGC9 are key Ca^{2+} channels for constitutive RH growth, while CNGC14ris a conditional Ca^{2+} channel in RH growth, given that the defective RH growth phenotypes exposed to air mainly result from simultaneous mutations in CNGC5, CNGC6, and CNGC9 (Figure 1; Supplemental Figures 3 and 4).

CNGC5, CNGC6, and CNGC9 Are Involved in Auxin Signaling in RHs

Cyclic nucleotides (cAMP and cGMP) are well characterized as the activators of mammalian cyclic nucleotide-gated channels, which are the orthologs of *Arabidopsis* CNGCs in mammalian cells. However, it took decades to confirm the presence of cAMP and cGMP and to identify the enzymes responsible for the synthesis and breakdown of the small molecules in plants (Raji and Gehring, 2017). cAMP and cGMP at the femtomolar level have been detected in pollen tubes, which are polar growth plant cells similar to RHs (Tunc-Ozdemir et al., 2013). We thus analyzed the effect of cAMP and cGMP on RH growth by adding either 1 μM cAMP or 1 μM cGMP in medium. However, no obvious effect of the two compounds was observed in RH growth and initiation in *shrh1* mutant and wild type (data not shown). It is well known that the initiation and growth of RHs are strongly regulated by auxin, ethylene, and ion nutrient availability. Of these factors, auxin is a dominant stimulating signal for RH initiation and growth (Grierson et al., 2014). To investigate whether CNGC5, CNGC6, and CNGC9 functioned as key components of the auxin signaling pathway in RH growth, we analyzed the effects of indole-3-acetic acid (IAA) and the auxin biosynthesis inhibitor yucasin (Nishimura et al., 2014) on RHs exposed to the air. Either IAA (0.05 μM) or yucasin (50 μM) was added to the solid medium. The experimental results demonstrated that RH growth was significantly promoted upon the application of 0.05 μM external IAA, but was significantly inhibited upon the application of 50 μM external yucasin in *shrh1*, wild type, *CNGC9-COM15*, and *CNGC9-OE42* to a similar extent without significant difference (Figure 7A and 7B; Supplemental Table 1). The RH branching rate was significantly increased by IAA and significantly reduced by yucasin in *shrh1* mutant relative to control conditions (Figure 7C). However, we did not observe an obvious change in the rupturing rate upon the application of either auxin or yucasin in wild type, *CNGC9-COM15*, and *CNGC9-OE42* (data not shown). RH density was significantly increased by auxin compared with control conditions to a similar extent in all genotypes, but was not obviously altered by yucasin relative to control (Figure 7D). These data suggest that CNGC5, CNGC6, and CNGC9 are also involved in RH initiation, and play a role in maintaining the integrity of RHs from bursting. However, it remains unclear whether auxin stimulates RH elongation via CNGC5, CNGC6, and CNGC9.

DISCUSSION

CNGC-Mediated External Ca^{2+} Influx Matters for RH Development

Cytosolic Ca^{2+} elevation and ROS production can be observed during the bulge formation in epidermis (Wymer et al., 1997;

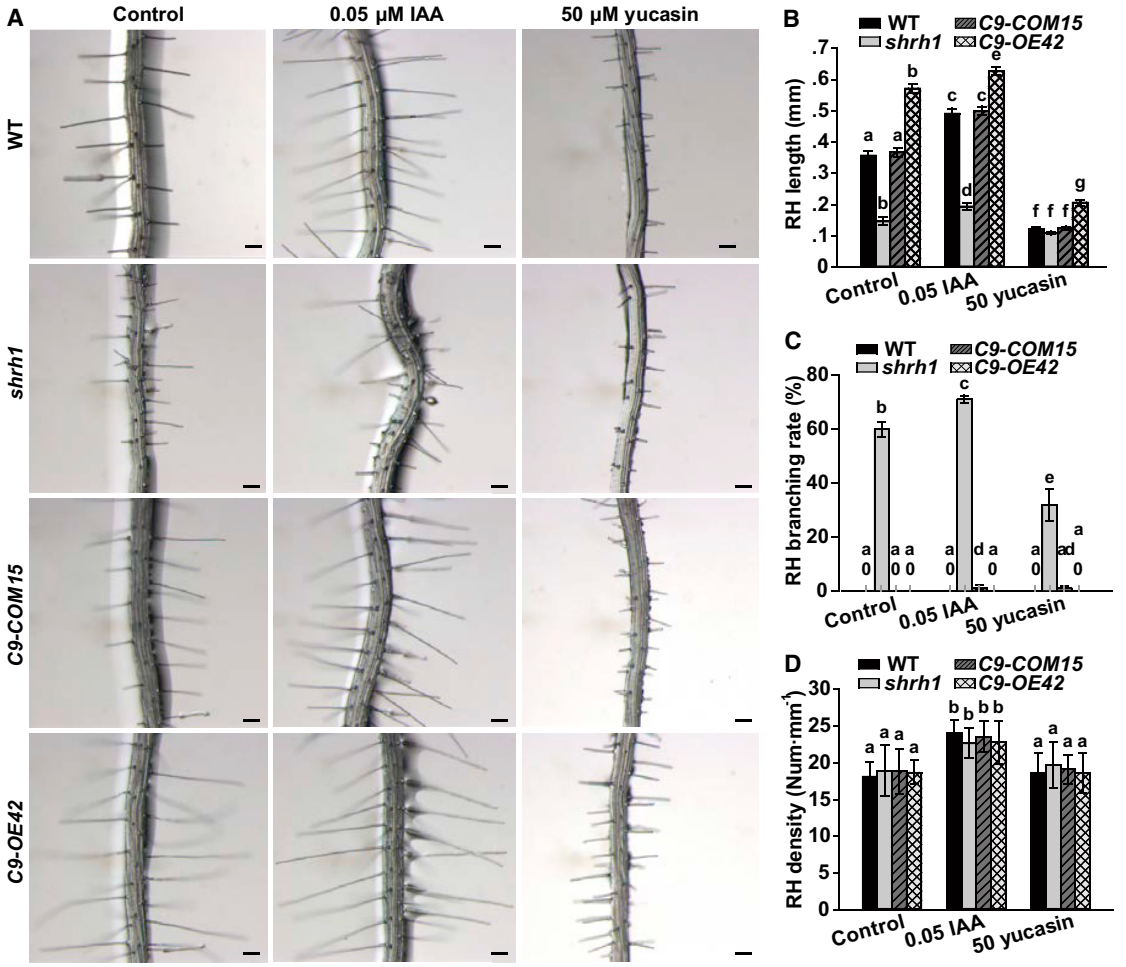

Figure 7. CNGC5, CNGC6, and CNGC9 Are Involved in Auxin Signaling in RHs.

(A) Typical roots and hairs. Scale bars, 0.1 mm.

(B–D) Statistical analysis of length **(B)**, branching rate **(C)**, and density **(D)** of RHs. No less than 30 roots and 200 RHs (7–10 RHs per root) were counted for each analysis of each line. Error bars depict means ±SEM. Samples with different letters are significantly different with $P < 0.05$ (Kruskal–Wallis one-way ANOVA).

Foreman et al., 2003). ROS production is required, and cytosolic Ca^{2+} elevation is believed to be not essential for RH initiation (Wymer et al., 1997; Foreman et al., 2003), implying that the Ca^{2+} channels responsible for Ca^{2+} influx are not essential for RH initiation. The single mutant *cngc14* can form normal RHs in air (Zhang et al., 2017). The triple mutant *cngc6cngc9cngc14* can form irregular bulges, but cannot form any RHs in their experimental condition (Brost et al., 2019). We show here that the triple mutant *shrh1* and quadruple mutant *shrh2* can form normal, but shorter RHs, regardless of whether the roots and hairs are exposed to air or embedded in solid medium (Figures 1 and 6), and RH density is not obviously altered in the triple and quadruple mutant compared with wild type under our experimental conditions (Supplemental Figures 3B and 8). It seems that all the studies from different groups support the conclusion that cytosolic Ca^{2+} evaluation is not indispensable for RH initiation/bulge or swelling formation. However, RH density was slightly reduced by the absence of external Ca^{2+} and increased by high external Ca^{2+} (15 mM) (Figure 2D), implying that CNGC5, CNGC6, and CNGC9 are involved in RH initiation. The irregular bulges in the triple mutant *cngc6cngc9cngc14* (Brost et al., 2019) also support a role of CNGC6, CNGC9, and CNGC14 in RH initiation. Swelling formation in epidermis is a process of cytoplasmic restructuring, which may not require the elevation of cytosolic Ca^{2+}. However, cytosolic Ca^{2+} elevation during RH initiation could be required by RH-elongating growth because the Ca^{2+} elevation during RH initiation is a start of establishment of the cytosolic Ca^{2+} gradient and RH-elongating growth. Thus, the two stages of RH development have an overlap. Some of Ca^{2+}-sensitive proteins involved in RH initiation may be affected by the changes in cytosolic Ca^{2+} level, and bulge formation can be consequently affected. This could be a side effect of Ca^{2+} on RH initiation under extremely low or high cytosolic Ca^{2+} conditions because of the overlap between the two stages of RH development. Thus, the three CNGCs as well as their redundant partners could be somehow involved in RH initiation indirectly.

Different RH-related phenotypes were observed in *cngc* mutants by different groups (Figures 1, 2, 5 and 6) (Zhang et al., 2017; Brost et al., 2019), supporting an indispensable role of the

multiple CNGC members for RH-elongating growth, not RH initiation. We revealed here that CNGC5, CNGC6, and CNGC9 are involved in RH growth by establishing and maintaining a sharp cytosolic Ca^{2+} gradient as well as regulating the oscillation of cytosolic Ca^{2+} in RH tips in *Arabidopsis*. Nevertheless, it is clear that the three CNGCs do matter for RH development, including RH initiation and elongating growth. In these processes, the three *Arabidopsis* CNGCs plus CNGC14 may form heterotetramers in RHs, as reported in *Lotus japonicus* (Chiasson et al., 2017), to form plastic Ca^{2+} channels for dynamic regulation of the channel activity at the post-translational level. Further investigations are needed to dissect the molecular mechanism underlying the channel activity regulation in RH growth.

Possible Processes of External Ca^{2+} Supply for RH Growth

It has been widely believed that the influx of external Ca^{2+} through Ca^{2+} channels at RH tips is the main source of Ca^{2+} for cytosolic Ca^{2+} gradients and RH growth. When roots are grown in medium or soil, Ca^{2+} in RHs is presumably absorbed directly from liquid medium or rhizosphere. However, RHs can grow normally in air, where the external Ca^{2+} supply seems to be absent. Two possibilities have been proposed for the supply of external Ca^{2+} to RHs (Ryan et al., 2001). First, RHs create their own internal Ca^{2+} gradients independent of external Ca^{2+}. Ca^{2+} may be provided by roots through RH's neighboring cells. The Ca^{2+} could be coated in vesicles. The vesicles travel inside the RHs to the RH apex to release Ca^{2+} to form a Ca^{2+} gradient. Second, external Ca^{2+} diffuses along the hydrated external surface of RHs to the external space close to RH tips, and then enters RHs through the inward Ca^{2+} channels. There is also a third possibility: the vesicles containing a large amount of Ca^{2+} may travel inside RHs to RH tips, the vesicle membrane and plasma membrane are fused at RH tips, and Ca^{2+} is then secreted to the extracellular space by exocytosis. External Ca^{2+} enters RHs through the inward Ca^{2+} channels composed of the CNGCs, no matter where the external Ca^{2+} comes from. The inward rectification of the three CNGCs as Ca^{2+} channels and the RH-related defects in a series of *cngc* mutants (Figures 1, 2, 5 and 6; Supplemental Figures 3, 4, and 6) (Gao et al., 2016; Zhang et al., 2017; Brost et al., 2019) strongly supports the last two possibilities, i.e., RHs take in Ca^{2+} from extracellular space via Ca^{2+} channel-mediated Ca^{2+} influx. Further analyses are required to clarify the exact process of external Ca^{2+} supply for RH growth.

RH development is regulated by an intrinsic sophisticated regulatory network in response to multiple phytohormones and various environmental stimuli(Cui et al., 2017). A large number of components, including transcriptional factors, ROPs, cytoskeleton, and Ca^{2+}, are involved in regulating RH development. This study and previous reports from other groups clearly show that Ca^{2+} channels composed of CNGCs and annexin1 are critical for RH growth (Laohavisit et al., 2012; Zhang et al., 2017; Brost et al., 2019). Thus, Ca^{2+} channels could be the core components of the regulatory networks underlying RH development. Further studies are needed to unravel how the multiple Ca^{2+} channels are integrated with other components of the network in regulation of RH development.

METHODS

Plant Growth

Arabidopsis plants (Columbia-0 ecotype) were grown in a growth room with a daily cycle of 16-h light/8-h darkness at 21°C ± 1°C as described by Zhang et al. (2016). *Arabidopsis* T-DNA insertion lines, SALK_149893 (*cngc5-1*), SALK_042207 (*cngc6-2*), SALK_026086 (*cngc9-1*), and SALK_206460C (*cngc14-1*), were obtained from the Arabidopsis Biological Resource Center.

Generation of Transgenic *Arabidopsis* Lines

For the generation of transgenic lines for the GUS staining assay, 20 GUS reporter vectors for *CNGC1* to *CNGC20* were prepared in pCambia1301P0G. Genomic DNA 2 kb upstream of the CNGCs' coding regions (native promoters) was fused to a GUS reporter gene, and the fused sequences were cloned into pCambia1301P0G vector. Transformation of wild-type *Arabidopsis* plants was carried out using the *Agrobacterium* (strain GV3101)-mediated floral dip method (Clough and Bent, 1998). T2 seedlings with hygromycin B resistance were selected for GUS staining assay.

For the generation of rescued lines in the background of *shrh1*, the full-length cDNAs of *CNGC5*, *CNGC6*, and *CNGC9* were PCR amplified and cloned in the vector pCambia1305 downstream of their respective native promoters. For the generation of OE lines in wild-type background, eGFP was fused to the N terminus of CNGC5, CNGC6, and CNGC9. The full-length cDNAs of the three fused proteins were cloned downstream of an *Ubiquitin10* promoter in the pCambia1305 vector, respectively. These vectors were then transformed into either *shrh1* mutant or wild-type plants using the *Agrobacterium*-mediated floral dip method (Clough and Bent, 1998). Homozygous lines from T3 generation were selected for experiments. *eGFP* was transformed into *shrh1* mutant and wild-type plants, and the transgenic lines selected from T3 generation were used as control plants in experiments. Primers and restriction sites for vector construction are listed in Supplemental Table 2.

GUS Staining Assay

Four-day-old T2 seedlings were incubated overnight in GUS staining buffer containing 100 mM Na_2HPO_4, 100 mM NaH_2PO_4, 5 mM EDTA–Na_2 (pH 8.0), 2 ml/l Triton X-100, 2.5 mM $K_3Fe(CN)_6$, 2.5 mM $K_4Fe(CN)_6$, and 0.5 mg/ml X-Gluc (PhytoTech) in a chamber at 37°C, then cleared in 70% ethanol. Images were captured under a stereo microscope (Model M205 FCA, Leica, Germany) using the software Leica Application Suite X (Leica).

RH Phenotype Analysis

Arabidopsis seeds were surface sterilized with 0.5% sodium hypochlorite for 10 min, washed three times with sterile water, and sowed in a Petri dish containing solid medium modified from a previous method (Zhao et al., 2016). The Ca^{2+}-free solid medium contained 5 mM KNO_3, 1 mM $MgSO_4$, 1 mM KH_2PO_4, 0.1 mM NaFeEDTA, 5 mM 2-(*N*-morpholino) ethanesulfonic acid (MES), 1% (w/v) sucrose, 0.68% (w/v) agarose, MS microelements at full strength, and pH 6.0 adjusted with Tris–Cl. $CaCl_2$ was added to the Ca^{2+}-free medium as indicated for Ca^{2+}-related RH phenotype analysis. K^+-free solid medium contained 3 mM NH_4NO_3, 1.5 mM $MgSO_4$, 1.25 mM $NH_4H_2PO_4$, 3 mM $CaCl_2$, 5 mM MES, 1% (w/v) sucrose, 0.68% (w/v) agarose, MS microelements at full strength, and pH 6.0 adjusted with Tris–Cl. KCl was added to K^+-free medium as indicated for K^+-related RH phenotype analysis. Pictures were taken under the Leica stereo microscope 4–5 days after seed sowing.

For the analysis of RHs exposed to air, seeds were sown on the surface of solid medium in the Petri dishes, which were then vertically placed in a growth room as described by Zhang et al. (2016). Roots grew on the surface of the solid medium, and most RHs were exposed to air under these conditions. For the measurement of RH length, roots and RHs

were covered by a coverglass to push the RHs down to an angle being basically parallel to the surface of solid medium for the convenience of RH phenotype analysis. For the analysis of RHs embedded in solid medium, seeds were sown on the surface of the solid medium and pushed into the solid medium using a sharp pipette tip. The Petri dishes were placed vertically in a growth room, and all roots and RHs grew in the solid medium under this condition. Pictures were taken under the Leica stereo microscope. The length, diameter, branching, and rupturing phenotypes of RHs were analyzed using the image software Digimizer (https://www.digimizer.com/index.php) after pictures were taken. RHs located within the 2-mm RHZ (Supplemental Figure 3E) were counted in RH-related phenotype analysis. For RH diameter measurements, the RH diameter at the region about 10 μm from RH tips was measured. For the measurements of the diameter of RH initiation area, the bulge-forming region of RHs was measured. RHs or bulges of epidermis less than 10 μm were categorized into initiating RHs, and not counted as RHs in the RH phenotype analysis. No less than 30 roots and 200 RHs (7–10 RHs per root) were analyzed for each *Arabidopsis* line analyzed. Statistical analysis was performed as described previously (Kolar and Senkova, 2008; Dang et al., 2018).

Time-Lapse Analysis of RH Growth

Time-lapse experiments in bright field in intact growing roots and hairs were conducted to monitor the growth, calculate the growth rate, and measure the growth time of RHs. Four-day-old seedlings grown in a Petri dish placed vertically in a growth room after seeds were sown on the surface of solid medium were used for the experiments. RHIZ of the seedlings with emerging and elongating RHs were selected for the experiments. A Petri dish was placed horizontally on the stage of a stereo microscope (Model M205 FCA; Leica, Germany). A set of optical sectioning images along *z* axis with a 22.5-μm step was captured each 1 min for no less than 300 min at room temperature (25°C ± 1°C) using a Sequential Frame Scan Mode following manufacturer's instructions (Leica). Each set of optical sections was composed of 15 sections for *shrh1* mutant and 21 sections for wild type, and was merged automatically and immediately to a single bright-field picture after the acquisition of the set of optical sections. Software Leica Application Suite X (Leica) was used for data acquisition and analysis.

RT–PCR and qRT–PCR

Arabidopsis seeds were sown on a plate containing solid medium as described above, and roots were cut off from the four-day-old seedlings and ground using a commercial electro drill in liquid nitrogen. Total RNA was extracted from the ground mix using TRIzol reagent (Invitrogen), and reverse transcriptions were performed with a TransScript One-Step gDNA Removal and cDNA Synthesis SuperMix kit (Transgen). The qRT–PCR analysis was conducted using a TransStart Top Green qPCR SuperMix kit (Transgen) on a Bio-Rad CFX Connect Real-Time PCR System according to the manufacturer's protocols (Wang et al., 2013). Primers are listed in Supplemental Table 2.

Subcellular Localization Assay

Arabidopsis OE lines were used for protein subcellular localization analysis of CNGC5, CNGC6, and CNGC9. Roots of four-day-old seedlings were cut off and placed on a slide. Four-day-old seedlings were immersed in FM4-64 solution (2 μM) for plasma membrane staining for 12 min, and FM4-64 fluorescent pictures were captured 10 min afterward. eGFP and FM4-64 fluorescent images of roots and RHs were taken under a Leica TCS SP8 STED 3X Super-Resolution Confocal Microscope (Leica, Germany). The fluorescence distribution was analyzed using the free software ImageJ2X.

HEK293T Cell Culturing

HEK293T cells were cultured in Dulbecco's modified Eagle's medium (DMEM; Gibco) supplemented with 10% fetal bovine serum (Gibco) and 100 IU/ml penicillin–streptomycin (Yeasen) in a water-injected incubator (Thermo, USA) with 5% CO_2 at 37°C in a moist atmosphere as described by Gao et al. (2016).

Patch-Clamp Experiments

For patch-clamp experiments in HEK293T cells, the CDS of *CNGC5* and *CNGC6* were fused upstream of *eGFP* sequences with an *IRES* linker (Mizuguchi et al., 2000) and constructed into pCI-neo vector under a *T7* promoter, respectively. HEK293T cells were transfected with vectors using a Lipofectamine 2000 Transfection Reagent kit (Invitrogen, USA) in penicillin–streptomycin-free DMEM as described by Gao et al. (2016). Plasmids for HEK293T transfection were extracted from *Escherichia coli* (DH5α) using a QIAGEN Plasmid Midi kit. HEK293T cells of a similar size showing bright eGFP fluorescence were used for patch-clamp experiments, and the HEK293T cells expressing *eGFP* were used as mock control.

The standard bath solution contained 120 mM NaCl, 10 mM $CaCl_2$, 10 mM CsCl, 2 mM $MgCl_2$, 10 mM glucose, and 10 mM HEPES (pH 7.2 adjusted with NaOH). $NMDG^+$-based bath solution was derived from standard bath solution by substituting 120 mM NaCl with 120 mM NMDG–Cl, and pH was adjusted to 7.2 with HCl. The standard pipette solution contained 120 mM Cs-glutamate, 8 mM NaCl, 2 mM $MgCl_2$, 3.35 mM $CaCl_2$, 6.7 mM EGTA, and 10 mM HEPES (pH 7.2 adjusted with CsOH). The osmolality of bath and pipette solutions was adjusted to 313 mmol/kg with D-glucose.

Whole-cell patch-clamp experiments were conducted using an Axopatch-200B patch-clamp setup (Axon Instruments, CA, USA) with a Digita-ta1440A digitizer combined with an inverted microscope (Model A1; Carl Zeiss, Germany). pClamp10.2 software (Axon Instruments) was used for data acquisition and analysis. A glass pipette was prepared with a glass capillary puller (Model PC-10; Narishige, Japan) and polished using a micro-forge (Model MF-830; Narishige). A membrane ramp protocol with 2-s duration from −180 mV to +20 mV was applied each 10 s for whole-cell current recordings in HEK293T cells as described by Gao et al. (2014).

Ca^{2+} Imaging

$[Ca^{2+}]_{cyt}$ in HEK293T cells and RHs was FRET/CFP imaged (Swanson and Gilroy, 2013) using a 40×, 1.3 numerical aperture, oil-immersion, Fluar objective under an inverted microscope (Model D1; Carl Zeiss, Germany). Samples were excited by a xenon light through a 430-nm excitation filter with 24-nm bandpass. CFP emission through a 470-nm emission filter with 24-nm bandpass and FRET-dependent emission through a 535-nm emission filter with 30-nm bandpass were captured by a Neo sCMOS CCD camera (Andor, UK). The excitation filter and emission filters were mounted in an excitation filter wheel (Lambda XL; Sutter Instrument, USA) and an emission filter wheel (Lambda XL; Sutter Instrument), respectively. Ratio florescence imaging software MetaFluor (version 7.8.0.0; Molecular Devices, USA) was used for data acquisition and analysis. A set of fluorescent and bright-field pictures were captured every 2 s, and the FRET/CFP ratio of interested regions was simultaneously calculated and recorded on the hard drive of a computer using the software MetaFluor. Exposure time to excitation light was 50 ms.

For Ca^{2+} imaging in HEK293T cells, the coding sequences of Ca^{2+} indicator YC3.6 were cloned into pCI-neo at the XhoI/NotI site, and were used for HEK293T transfection and cytosolic Ca^{2+} ($[Ca^{2+}]_{cyt}$) imaging. HEK293T cells were transfected in penicillin–streptomycin-free DMEM as described by Gao et al. (2014). HEK293T cells were digested with 0.25% trypsin–EDTA, collected by centrifugation at 1000 rpm for 1 min, and resuspended in Ca^{2+}-free incubation buffer (CIB) containing 130 mM NaCl, 3 mM KCl, 0.6 mM $MgCl_2$, 1.2 mM $NaHCO_3$, 10 mM glucose, and 10 mM HEPES, at pH 7.2 adjusted with NaOH. HEK293T cells showing bright YC3.6 fluorescence were used for $[Ca^{2+}]_{cyt}$ imaging. Cytosolic Ca^{2+} was analyzed by monitoring the ratio

of FRET/CFP in CIB solution at room temperature (25°C ± 1°C) under the Zeiss inverted microscope (Model D1). External Ca^{2+} (10 mM) was added as indicated.

For $[Ca^{2+}]_{cyt}$ imaging in *Arabidopsis* RHs, the *shrh1* plants were crossed with wild-type plants expressing *YC3.6* under a *35S* promoter, and homozygous *shrh1* mutant with strong YC3.6 fluorescent signal was isolated from progeny for further experiments. FRET/CFP-based $[Ca^{2+}]_{cyt}$ imaging was performed in RHs of four-day-old seedlings adhered to a coverglass with medical adhesive glue (Hollister, USA). The coverglass was immersed in a chamber containing working solution (5 mM KCl, 100 μM $CaCl_2$, 10 mM MES–Tris [pH 5.7]). *In situ* calibration was performed as described by Swanson and Gilroy (2013). The Ca^{2+} saturating FRET/CFP ratio for YC3.6 (R_{max}) was recorded upon the application of 5 mM $CaCl_2$ and 20 μM Ca^{2+} ionophore Br-A23187, and the minimum FRET/CFP ratio (R_{min}) was recorded upon the application of 20 μM Br-A23187 and 5 mM EGTA. The estimated $[Ca^{2+}]_{cyt}$ value was calculated according to the equation $[Ca^{2+}]_{cyt} = (K_D[R - R_{min}]/[R_{max} - R])^{1/n}$, where R is the measured ratio value, K_D is 250 nM for YC3.6, and the Hill coefficient n is determined as one for YC3.6 as reported by Nagai et al. (2004).

SUPPLEMENTAL INFORMATION

Supplemental Information is available at *Plant Communications Online*.

A video abstract is available at https://doi.org/10.1016/j.xplc.2019.100001#mmc2.

FUNDING

This work was supported by the Strategic Priority Research Program of the Chinese Academy of Sciences (XDB27020102) and the National Natural Science Foundation of China (91635301, 31570262, and 31770292).

AUTHOR CONTRIBUTIONS

Investigation, Y.-Q.T., Y.Y., L.-L.G., S.-J.S., A.Z., and C.-F.F.; Methodology, W.X., L.W., and H.L.; Funding Acquisition, Supervision, and Writing, Y.-F.W.

ACKNOWLEDGMENTS

We thank Yunxiao He for assistance in confocal imaging experiments, Hongjie Wu (Focell) for assistance in cytosolic Ca^{2+} imaging experiments, and Hong-Wei Xue (Shanghai Jiao Tong University) for providing IAA and yucasin. No conflict of interest declared.

Received: August 2, 2019
Revised: August 6, 2019
Accepted: August 23, 2019
Published: September 4, 2019

REFERENCES

Akiyama, H., and Kamiguchi, H. (2015). Second messenger networks for accurate growth cone guidance. Dev. Neurobiol. **75**:411–422.

Baluska, F., Salaj, J., Mathur, J., Braun, M., Jasper, F., Samaj, J., Chua, N.H., Barlow, P.W., and Volkmann, D. (2000). Root hair formation: F-actin-dependent tip growth is initiated by local assembly of profilin-supported F-actin meshworks accumulated within expansin-enriched bulges. Dev. Biol. **227**:618–632.

Berger, F., Haseloff, J., Schiefelbein, J., and Dolan, L. (1998). Positional information in root epidermis is defined during embryogenesis and acts in domains with strict boundaries. Curr. Biol. **8**:421–430.

Bernhardt, C., Lee, M.M., Gonzalez, A., Zhang, F., Lloyd, A., and Schiefelbein, J. (2003). The bHLH genes *GLABRA3* (*GL3*) and *ENHANCER OF GLABRA3* (*EGL3*) specify epidermal cell fate in the *Arabidopsis* root. Development **130**:6431–6439.

Bernhardt, C., Zhao, M., Gonzalez, A., Lloyd, A., and Schiefelbein, J. (2005). The bHLH genes *GL3* and *EGL3* participate in an intercellular regulatory circuit that controls cell patterning in the *Arabidopsis* root epidermis. Development **132**:291–298.

Bibikova, T.N., Blancaflor, E.B., and Gilroy, S. (1999). Microtubules regulate tip growth and orientation in root hairs of *Arabidopsis thaliana*. Plant J. **17**:657–665.

Bibikova, T.N., Jacob, T., Dahse, I., and Gilroy, S. (1998). Localized changes in apoplastic and cytoplasmic pH are associated with root hair development in *Arabidopsis thaliana*. Development **125**:2925–2934.

Bibikova, T.N., Zhigilei, A., and Gilroy, S. (1997). Root hair growth in *Arabidopsis thaliana* is directed by calcium and an endogenous polarity. Planta **203**:495–505.

Brost, C., Studtrucker, T., Reimann, R., Denninger, P., Czekalla, J., Krebs, M., Fabry, B., Schumacher, K., Grossmann, G., and Dietrich, P. (2019). Multiple cyclic nucleotide-gated channels coordinate calcium oscillations and polar growth of root hairs. Plant J. **99**:910–923.

Carol, R.J., and Dolan, L. (2006). The role of reactive oxygen species in cell growth: lessons from root hairs. J. Exp. Bot. **57**:1829–1834.

Carol, R.J., Takeda, S., Linstead, P., Durrant, M.C., Kakesova, H., Derbyshire, P., Drea, S., Zarsky, V., and Dolan, L. (2005). A RhoGDP dissociation inhibitor spatially regulates growth in root hair cells. Nature **438**:1013.

Chiasson, D.M., Haage, K., Sollweck, K., Brachmann, A., Dietrich, P., and Parniske, M. (2017). A quantitative hypermorphic CNGC allele confers ectopic calcium flux and impairs cellular development. eLife **6**:e25012.

Clough, S.J., and Bent, A.F. (1998). Floral dip: a simplified method for Agrobacterium-mediated transformation of *Arabidopsis thaliana*. Plant J. **16**:735–743.

Cui, S., Suzaki, T., Tominaga-Wada, R., and Yoshida, S. (2017). Regulation and functional diversification of root hairs. Semi. Cell Dev. Biol. **83**:115–122.

Dang, X., Yu, P., Li, Y., Yang, Y., Zhang, Y., Ren, H., Chen, B., and Lin, D. (2018). Reactive oxygen species mediate conical cell shaping in *Arabidopsis thaliana* petals. PLoS Genet. **14**:e1007705.

Demidchik, V., Bowen, H.C., Maathuis, F.J.M., Shabala, S.N., Tester, M.A., White, P.J., and Davies, J.M. (2002). *Arabidopsis thaliana* root non-selective cation channels mediate calcium uptake and are involved in growth. Plant J. **32**:799–808.

Di Cristina, M., Sessa, G., Dolan, L., Linstead, P., Baima, S., Ruberti, I., and Morelli, G. (1996). The *Arabidopsis* Athb-10 (GLABRA2) is an HD-Zip protein required for regulation of root hair development. Plant J. **10**:393–402.

Duan, Q., Kita, D., Li, C., Cheung, A.Y., and Wu, H.-M. (2010). FERONIA receptor-like kinase regulates RHO GTPase signaling of root hair development. Proc. Natl. Acad. Sci. USA **107**:17821–17826.

Felle, H.H., and Hepler, P.K. (1997). The cytosolic Ca^{2+} concentration gradient of *Sinapis alba* root hairs as revealed by Ca^{2+}-selective microelectrode tests and fura-dextran ratio imaging. Plant Physiol. **114**:39–45.

Feske, S., Gwack, Y., Prakriya, M., Srikanth, S., Puppel, S.H., Tanasa, B., Hogan, P.G., Lewis, R.S., Daly, M., and Rao, A. (2006). A mutation in Orai1 causes immune deficiency by abrogating CRAC channel function. Nature **441**:179–185.

Foreman, J., Demidchik, V., Bothwell, J.H., Mylona, P., Miedema, H., Torres, M.A., Linstead, P., Costa, S., Brownlee, C., Jones, J.D., et al. (2003). Reactive oxygen species produced by NADPH oxidase regulate plant cell growth. Nature **422**:442–446.

Gao, Q.-F., Fei, C.-F., Dong, J.-Y., Gu, L.-L., and Wang, Y.-F. (2014). *Arabidopsis* CNGC18 is a Ca^{2+}-permeable channel. Mol. Plant **7**:739–743.

Gao, Q.-F., Gu, L.-L., Wang, H.-Q., Fei, C.-F., Fang, X., Hussain, J., Sun, S.-J., Dong, J.-Y., Liu, H., and Wang, Y.-F. (2016). Cyclic nucleotide-gated channel 18 is an essential Ca^{2+} channel in pollen tube tips for pollen tube guidance to ovules in *Arabidopsis*. Proc. Natl. Acad. Sci. USA **113**:3096–3101.

Grierson, C., Nielsen, E., Ketelaarc, T., and Schiefelbein, J. (2014). Root hairs. The Arabidopsis Book **12**:e0172.

Gu, L.-L., Gao, Q.-F., and Wang, Y.-F. (2017). Cyclic nucleotide-gated channel 18 functions as an essential Ca^{2+} channel for pollen germination and pollen tube growth in *Arabidopsis*. Plant Signal Behav **12**:e1197999.

Guan, Y., Guo, J., Li, H., and Yang, Z. (2013). Signaling in pollen tube growth: crosstalk, feedback, and missing links. Mol. Plant **6**:1053–1064.

Herrmann, A., and Felle, H.H. (1995). Tip growth in root hair cells of *Sinapis alba* L.: significance of internal and external Ca^{2+} and pH. New Phytol. **129**:523–533.

Huang, G.Q., Li, E., Ge, F.R., Li, S., Wang, Q., Zhang, C.Q., and Zhang, Y. (2013). *Arabidopsis* RopGEF4 and RopGEF10 are important for FERONIA-mediated developmental but not environmental regulation of root hair growth. New Phytol. **200**:1089–1101.

Hung, C.Y., Lin, Y., Zhang, M., Pollock, S., Marks, M.D., and Schiefelbein, J. (1998). A common position-dependent mechanism controls cell-type patterning and GLABRA2 regulation in the root and hypocotyl epidermis of *Arabidopsis*. Plant Physiol. **117**:73–84.

Ibáñez, F., Wall, L., and Fabra, A. (2017). Starting points in plant-bacteria nitrogen-fixing symbioses: intercellular invasion of the roots. J. Exp. Bot. **68**:1905–1918.

Jones, M.A., Shen, J.J., Fu, Y., Li, H., Yang, Z., and Grierson, C.S. (2002). The *Arabidopsis* Rop2 GTPase is a positive regulator of both root hair initiation and tip growth. Plant Cell **14**:763–776.

Ketelaar, T., Galway, M.E., Mulder, B.M., and Emons, A.M. (2008). Rates of exocytosis and endocytosis in *Arabidopsis* root hairs and pollen tubes. J. Microsc. **231**:265–273.

Kiegle, E., Gilliham, M., Haseloff, J., and Tester, M. (2000). Hyperpolarisation-activated calcium currents found only in cells from the elongation zone of *Arabidopsis thaliana* roots. Plant J. **21**:225–229.

Kirik, V., Simon, M., Huelskamp, M., and Schiefelbein, J. (2004). The *ENHANCER OF TRY AND CPC1* gene acts redundantly with *TRIPTYCHON* and *CAPRICE* in trichome and root hair cell patterning in *Arabidopsis*. Dev. Biol. **268**:506–513.

Kolar, J., and Senkova, J. (2008). Reduction of mineral nutrient availability accelerates flowering of *Arabidopsis thaliana*. J. Plant Physiol. **165**:1601–1609.

Konrad, K.R., Wudick, M.M., and Feijo, J.A. (2011). Calcium regulation of tip growth: new genes for old mechanisms. Curr. Opin. Plant Biol. **14**:721–730.

Laohavisit, A., Shang, Z., Rubio, L., Cuin, T.A., Véry, A.-A., Wang, A., Mortimer, J.C., Macpherson, N., Coxon, K.M., Battey, N.H., et al. (2012). *Arabidopsis* annexin1 mediates the radical-activated plasma membrane Ca^{2+}- and K^+-permeable conductance in root cells. Plant Cell **24**:1522–1533.

Lee, M.M., and Schiefelbein, J. (1999). WEREWOLF, a MYB-related protein in *Arabidopsis*, is a position-dependent regulator of epidermal cell patterning. Cell **99**:473–483.

Leng, Q., Mercier, R.W., Yao, W., and Berkowitz, G.A. (1999). Cloning and first functional characterization of a plant cyclic nucleotide-gated cation channel. Plant Physiol. **121**:753–761.

Leng, Q., Mercier, R.W., Hua, B.G., Fromm, H., and Berkowitz, G.A. (2002). Electrophysiological analysis of cloned cyclic nucleotide-gated ion channels. Plant Physiol. **128**:400–410.

Lin, Y., and Schiefelbein, J. (2001). Embryonic control of epidermal cell patterning in the root and hypocotyl of *Arabidopsis*. Development **128**:3697–3705.

Liszkay, A., van der Zalm, E., and Schopfer, P. (2004). Production of reactive oxygen intermediates ($O_2^{\cdot-}$, H_2O_2, and $^{\cdot}OH$) by maize roots and their role in wall loosening and elongation growth. Plant Physiol. **136**:3114–3123.

Miedema, H., Demidchik, V., Véry, A.-A., Bothwell, J.H.F., Brownlee, C., and Davies, J.M. (2008). Two voltage-dependent calcium channels co-exist in the apical plasma membrane of *Arabidopsis thaliana* root hairs. New Phytol. **179**:378–385.

Mizuguchi, H., Xu, Z., Ishii-Watabe, A., Uchida, E., and Hayakawa, T. (2000). IRES-dependent second gene expression is significantly lower than cap-dependent first gene expression in a bicistronic vector. Mol. Ther. **1**:376–382.

Molendijk, A.J., Bischoff, F., Rajendrakumar, C.S., Friml, J., Braun, M., Gilroy, S., and Palme, K. (2001). *Arabidopsis thaliana* Rop GTPases are localized to tips of root hairs and control polar growth. EMBO J. **20**:2779–2788.

Monshausen, G.B., Bibikova, T.N., Messerli, M.A., Shi, C., and Gilroy, S. (2007). Oscillations in extracellular pH and reactive oxygen species modulate tip growth of *Arabidopsis* root hairs. Proc. Natl. Acad. Sci. USA **104**:20996–21001.

Monshausen, G.B., Messerli, M.A., and Gilroy, S. (2008). Imaging of the yellow cameleon 3.6 indicator reveals that elevations in cytosolic Ca^{2+} follow oscillating increases in growth in root hairs of *Arabidopsis*. Plant Physiol. **147**:1690–1698.

Nagai, T., Yamada, S., Tominaga, T., Ichikawa, M., and Miyawaki, A. (2004). Expanded dynamic range of fluorescent indicators for Ca^{2+} by circularly permuted yellow fluorescent proteins. Proc. Natl. Acad. Sci. USA **101**:10554–10559.

Nishimura, T., Hayashi, K.-i., Suzuki, H., Gyohda, A., Takaoka, C., Sakaguchi, Y., Matsumoto, S., Kasahara, H., Sakai, T., Kato, J.-i., et al. (2014). Yucasin is a potent inhibitor of YUCCA, a key enzyme in auxin biosynthesis. Plant J. **77**:352–366.

Pei, W., Du, F., Zhang, Y., He, T., and Ren, H. (2012). Control of the actin cytoskeleton in root hair development. Plant Sci. **187**:10–18.

Raji, M., and Gehring, C. (2017). *In vitro* assessment of guanylyl cyclase activity of plant receptor kinases. In Plant Receptor Kinases: Methods and Protocols, R.B. Aalen, ed. (New York, NY: Springer New York), pp. 131–140.

Rerie, W.G., Feldmann, K.A., and Marks, M.D. (1994). The *GLABRA2* gene encodes a homeo domain protein required for normal trichome development in *Arabidopsis*. Genes Dev. **8**:1388–1399.

Rounds, C.M., and Bezanilla, M. (2013). Growth mechanisms in tip-growing plant cells. Ann. Rev. Plant Biol. **64**:243–265.

Ryan, E., Steer, M., and Dolan, L. (2001). Cell biology and genetics of root hair formation in *Arabidopsis thaliana*. Protoplasma **215**:140–149.

Schellmann, S., Schnittger, A., Kirik, V., Wada, T., Okada, K., Beermann, A., Thumfahrt, J., Jürgens, G., and Hülskamp, M. (2002). *TRIPTYCHON* and *CAPRICE* mediate lateral inhibition during trichome and root hair patterning in *Arabidopsis*. EMBO J. **21**:5036–5046.

Schiefelbein, J.W., Shipley, A., and Rowse, P. (1992). Calcium influx at the tip of growing root-hair cells of *Arabidopsis thaliana*. Planta **187**:455–459.

Sieberer, B.J., Ketelaar, T., Esseling, J.J., and Emons, A.M.C. (2005). Microtubules guide root hair tip growth. New Phytol. **167**:711–719.

Simon, M., Lee, M.M., Lin, Y., Gish, L., and Schiefelbein, J. (2007). Distinct and overlapping roles of single-repeat MYB genes in root epidermal patterning. Dev. Biol. **311**:566–578.

Swanson, S.J., and Gilroy, S. (2013). Imaging changes in cytoplasmic calcium using the yellow cameleon 3.6 biosensor and confocal microscopy. In Plant Lipid Signaling Protocols, T. Munnik and I. Heilmann, eds. (Totowa, NJ: Humana Press), pp. 291–302.

Tominaga, M., Kojima, H., Yokota, E., Nakamori, R., Anson, M., Shimmen, T., and Oiwa, K. (2012). Calcium-induced mechanical change in the neck domain alters the activity of plant myosin XI. J. Biol. Chem. **287**:30711–30718.

Tunc-Ozdemir, M., Tang, C., Ishka, M.R., Brown, E., Groves, N.R., Myers, C.T., Rato, C., Poulsen, L.R., McDowell, S., Miller, G., et al. (2013). A cyclic nucleotide-gated channel (CNGC16) in pollen is critical for stress tolerance in pollen reproductive development. Plant Physiol. **161**:1010–1020.

Urquhart, W., Chin, K., Ung, H., Moeder, W., and Yoshioka, K. (2011). The cyclic nucleotide-gated channels AtCNGC11 and 12 are involved in multiple Ca^{2+}-dependent physiological responses and act in a synergistic manner. J. Exp. Bot. **62**:3671–3682.

Véry, A.A., and Davies, J.M. (2000). Hyperpolarization-activated calcium channels at the tip of *Arabidopsis* root hairs. Proc. Natl. Acad. Sci. USA **97**:9801–9806.

Wada, T., Tachibana, T., Shimura, Y., and Okada, K. (1997). Epidermal cell differentiation in *Arabidopsis* determined by a *Myb* homolog, CPC. Science **277**:1113–1116.

Wada, T., Kurata, T., Tominaga, R., Koshino-Kimura, Y., Tachibana, T., Goto, K., Marks, M.D., Shimura, Y., and Okada, K. (2002). Role of a positive regulator of root hair development, *CAPRICE*, in *Arabidopsis* root epidermal cell differentiation. Development **129**:5409–5419.

Walker, A.R., Davison, P.A., Bolognesi-Winfield, A.C., James, C.M., Srinivasan, N., Blundell, T.L., Esch, J.J., Marks, M.D., and Gray, J.C. (1999). The TRANSPARENT TESTA GLABRA1 locus, which regulates trichome differentiation and anthocyanin biosynthesis in *Arabidopsis*, encodes a WD40 repeat protein. Plant Cell **11**:1337–1350.

Wang, Y., Kang, Y., Ma, C., Miao, R., Wu, C., Long, Y., Ge, T., Wu, Z., Hou, X., Zhang, J., et al. (2017). CNGC2 is a Ca^{2+} influx channel that prevents accumulation of apoplastic Ca^{2+} in the leaf. Plant Physiol. **173**:1342–1354.

Wang, Y.F., Munemasa, S., Nishimura, N., Ren, H.M., Robert, N., Han, M., Puzorjova, I., Kollist, H., Lee, S., Mori, I., et al. (2013). Identification of cyclic GMP-activated nonselective Ca^{2+}-permeable cation channels and associated CNGC5 and CNGC6 genes in *Arabidopsis* guard cells. Plant Physiol. **163**:578–590.

Wymer, C.L., Bibikova, T.N., and Gilroy, S. (1997). Cytoplasmic free calcium distributions during the development of root hairs of *Arabidopsis thaliana*. Plant J. **12**:427–439.

Xu, J., Li, H.D., Chen, L.Q., Wang, Y., Liu, L.L., He, L., and Wu, W.H. (2006). A protein kinase, interacting with two calcineurin B-like proteins, regulates K^+ transporter AKT1 in *Arabidopsis*. Cell **125**:1347–1360.

Zhang, A., Ren, H.-M., Tan, Y.-Q., Qi, G.-N., Yao, F.-Y., Wu, G.-L., Yang, L.-W., Hussain, J., Sun, S.-J., and Wang, Y.-F. (2016). S-type anion channels SLAC1 and SLAH3 function as essential negative regulators for K^+ channel KAT1 and stomatal opening in *Arabidopsis*. Plant Cell **28**:949–965.

Zhang, S., Pan, Y., Tian, W., Dong, M., Zhu, H., Luan, S., and Li, L. (2017). *Arabidopsis* CNGC14 mediates calcium influx required for tip growth in root hairs. Mol. Plant **10**:1004–1006.

Zhao, S., Zhang, M.L., Ma, T.L., and Wang, Y. (2016). Phosphorylation of ARF2 relieves its repression of transcription of the K^+ transporter gene HAK5 in response to low potassium stress. Plant Cell **28**:3005–3019.